Supporting Information

Synergistyically Enhanced Iron and Zinc Bimetallic Sites as an Advanced ORR Electrocatalyst for Flow Liquid Rechargeable Zn-air Batteries

Zhi-Da Wang,[a] Song Liang,*[a] Cheng-Kun Bai,[a] Zhong-feng Guo,[a] Guo-Long Lu,[a] Hang Sun,[a] Zhen-Ning Liu *[a] and Hong-Ying Zang *[b]

[a] Key Laboratory of Bionic Engineering (Ministry of Education), College of Biological and Agricultural Engineering, Jilin University, Changchun, 130022, China. E-mail: Songliang@jlu.edu.cn; liu_zhenning@jlu.edu.cn
[b] Key Laboratory of Polyoxometalate Science of the Ministry of Education, Faculty of Chemistry, Northeast Normal University, Changchun, 130024, China. E-mail: zanghy100@nenu.edu.cn

Supplementary Text

Experimental section

Synthetic optimization

For comparison, the TA/Fe(III)/PI/MWCNTs was then carbonized at different temperatures (700 and 900 ℃), denoted as Fe-Zn/N/C/MWCNTs-700 and Fe-Zn/N/C/MWCNTs-900, respectively.

Besides, the TA/Fe(III)/PI/MWCNTs was then prepared at different amount of $Fe(NO_3)_3 \cdot 9H_2O$ (100, 200, and 300 mg), and subsequently carbonization in the same way, denoted as Fe-Zn/N/C/MWCNTs-800-100, Fe-Zn/N/C/MWCNTs-800-200, and Fe-Zn/N/C/MWCNTs-800-400, respectively.

Meanwhile, Fe-Zn/N/MWCNTs-800, Fe-Zn/C/MWCNTs-800, Fe-Zn/N/C-800, or Fe/N/C/MWCNTs-800 were also prepared without TA, PI, MWCNTs, or molten-salt, respectively.

Materials Characterization

The morphology, structure, and composition of materials in this paper were systematically characterized by methods of Fourier Transform Infrared Spectrometer (FT-IR, Shimadzu, IR Affinity-1), X-ray diffraction (XRD, Shimadzu, 6100), Raman spectroscopy with a LabRAM HR high-resolution Raman spectrometer (Horiba-Jobin Yvon), scanning electron microscopy (SEM, Hitachi, SU-70), transmission electron microscopy (TEM, JEOL, JEM-2100F), X-ray photoelectron spectroscopy (XPS, VG ESCALAB MKII, Al-Ka radiation), and inductively coupled plasma optical emission spectrometry (ICP-OES, Agilent 5110). The surface area, pore size, and pore-size distribution of the materials were measured by the Brunauer–Emmett–Teller (BET) nitrogen adsorption–desorption and Barrett–Joyner–Halenda (BJH) methods (ASAP 2020 M).

Electrochemical tests

The electrochemical experiments were carried out with a computer-controlled potentiostat (CHI 750E, Shanghai CH Instrument, China) using a three-electrode configuration with glassy carbon working electrode, graphite counter electrode, and corresponding reference electrode, respectively. An Ag/AgCl electrode (saturated KCl) was used as a reference electrode, a graphite plate was used as a counter electrode and the catalyst film coated a rotating ring-disk electrode (RRDE) with a glassy carbon disk (5.5 mm in diameter) and a Pt ring (inner/outer-ring diameter: 6.5/8.5 mm) were used as the working electrode, respectively.

Typically, 5 mg of catalyst was mixed with 50 μL of Nafion solution (5 wt%), 400 μL of isopropanol and 600 μL of DI water and sonicated for 30 mins to form a homogeneous ink. Then, 10 μL of the dispersion of homogeneous ink was loaded onto RRDE and dried naturally. For comparison, the Pt/C (20 wt% Pt) catalyst coated onto RRDE were used as the control group. The potentials were presented with respect to the reversible hydrogen electrode (RHE), E (RHE) = E (Ag/AgCl/saturated KCl) + 0.0591 pH + 0.197 in this paper.

All electrochemical measurements were performed at room temperature in 0.1 M KOH saturated with O_2 or Ar for 30 min prior to the experiment and the gas flow was maintained during tests. Cyclic voltammetry (CV) tests were performed at a scan rate of 10 $mV \cdot s^{-1}$. Linear sweep voltammetry (LSV) tests were run at a scan rate of 10 $mV \cdot s^{-1}$ at different rotation rates combined with the RRDE. The

apparent number of electrons transferred for ORR on the electrodes was also determined by the Koutecky-Levich equations given blow:

$$\frac{1}{J} = \frac{1}{J_L} + \frac{1}{J_K} = \frac{1}{B\omega^{1/2}} + \frac{1}{J_K} \qquad (1)$$

$$B = 0.62nFC_0(D_0)^{2/3}\upsilon^{-1/6} \qquad (2)$$

in which J is the measured current density, J_K and J_L are the kinetic and diffusion-limiting current densities, ω is electrode rotation rate, n is the overall number of electrons transferred in oxygen reduction, F is the Faraday constant (F = 96485 C mol^{-1}), C_0 is the bulk concentration of O_2, υ is the kinematic viscosity of the electrolyte, and k is the electron transfer rate constant. The number of electrons transferred (n) and J_K could be obtained from the slope and intercept of the Koutecky-Levich plots, respectively, and by using parameters C_0 = 1.2 ×10 $^{-6}$ mol cm^{-3}, D_0 = 1.9 × 10 $^{-5}$ cm^2 s^{-1}, and υ = 0.01 cm^2 s^{-1} in 0.1 M KOH, 25 ℃, 1 atm. For RRDE measurements, the curves were collected at a rotation rate of 1600 rpm.

For the Tafel slope, J_K was corrected through the diffusion current density (J_L) from the Koutecky-Levich equation by:

$$J_K = \frac{J_L \times J}{J_L - J} \qquad (3)$$

The H_2O_2% and the electron transfer number (n) were calculated as follows:

$$HO_2^-\% = 200 \times \frac{I_R/N}{I_D + I_R/N} \qquad (4)$$

$$n = \frac{4I_D}{I_D + I_R/N} \qquad (5)$$

where I_D is the disk current and I_R is the ring current, respectively, and N (0.37) is the collecting efficiency of the Pt ring.

The stability and methanol tolerance tests of the electrocatalysts were measured by chronoamperometric (CA) measurements with the potential holding at 0.5 V (*vs.* RHE) with a rotation rate of 1600 rpm in O_2-saturated corresponding solutions. CA measurements were also used to judge the stability of the catalyst. Methanol tolerance experiments were developed with CA measurements by adding 3 M methanol into O_2-saturated 0.1 M KOH at ca. 300 s.

To evaluate the OER catalytic activities of electrocatalysts, we used carbon paper as the working electrode substrate. In above ORR measurements, 200 μL of homogeneous ink was coated onto a piece of carbon paper (1 × 1 cm^2), and the amount of electrocatalysts on the carbon paper was about 1 mg·cm^{-2}. The LSV tests were run in a 6.0 M KOH solution. And the stability tests were performed by CA measurements with the potential holding at 1.587 V (*vs.* RHE) in a Teflon (PTFE) cell containing the 6.0 M solutions. The overpotential at 10 mA·cm^{-2} (η) was calculated as follows:

$$\eta = E_{10} - 1.23 \qquad (6)$$

where E_{10} is the OER polarization potential relative to the RHE at 10 mA·cm^{-2} and the O_2/H_2O equilibrium potential is suggested as 1.23 V.

All the electrochemical tests were carried out at ambient temperature.

Assembly of flow liquid Rechargeable Zn-air batteries

The home-made Zn-air battery was assembled to identify the performance of the Fe-Zn/N/C/MWCNTs-800 catalyst in practical applications. Briefly, a polished zinc plate was used as the anode, the electrocatalyst of Fe-Zn/N/C/MWCNTs-800 or 20% Pt/C (1.0 mg cm^{-2}) dispersed on the gas diffusion layer was used as the air cathode, and a solution of 6.0 M KOH containing 0.2 M $Zn(OAc)_2$ was used as the electrolyte, respectively. Besides, the flowing rate of the electrolyte could be easily controlled by a circulating pump at 3 mL min^{-1}. The CHI 750E and multi-channel battery testing system (Land CT 2001a) electrochemistry workstation were adopted to test the discharge/charge performance and cycling stability of the Zn-air batteries at room temperature. The blue light emitting diode (LED) screen and the single bulb pattern (about 3 V) were commercially available.

Supplementary Figures and captions

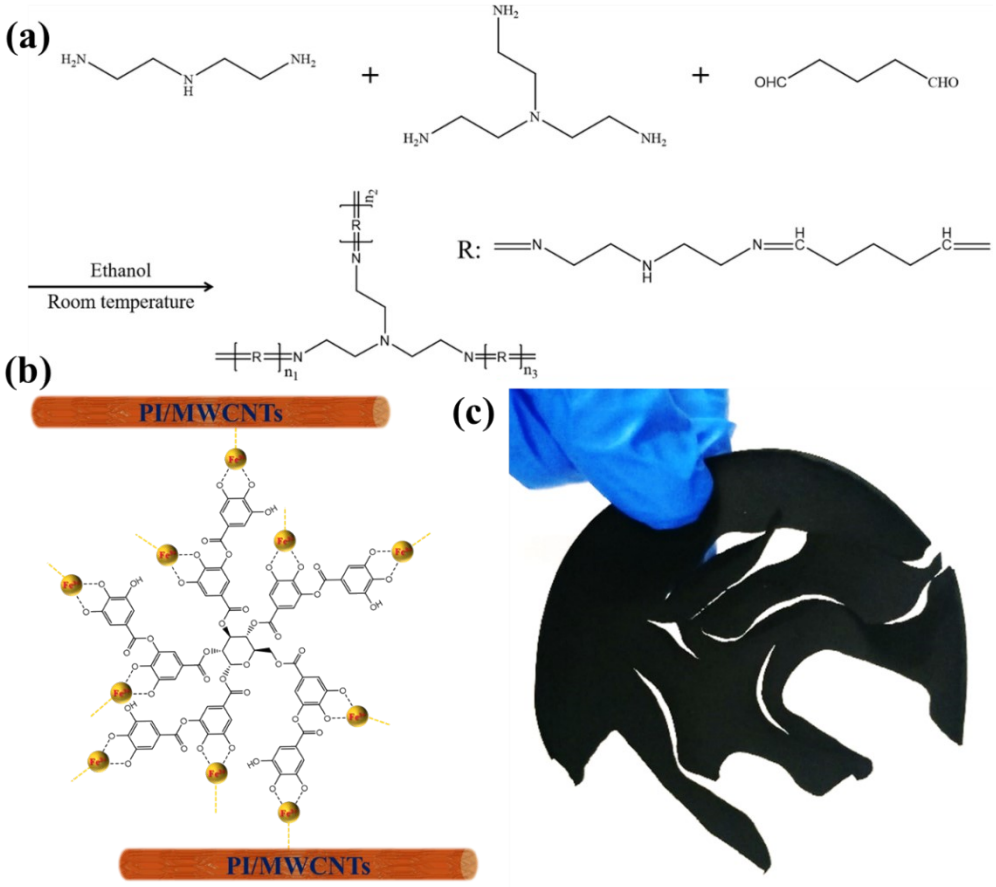

Fig. S1. (a) Schematic synthesis process of polyimine (PI). (b) The chemical structures and (c) the picture of TA-Fe-PI/MWCNTs composites.

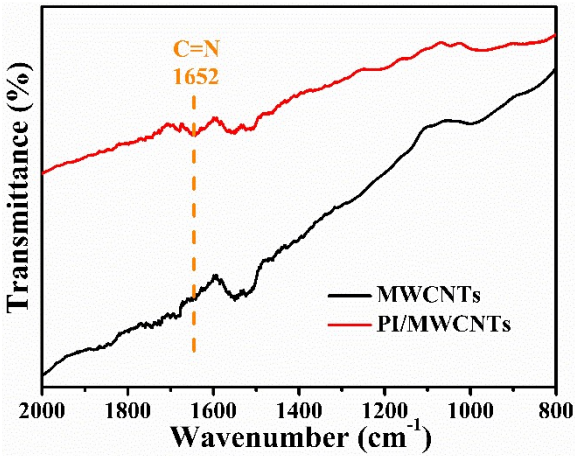

Fig. S2. FT-IR spectra of PI/MWCNTs composites and pure MWCNTs.

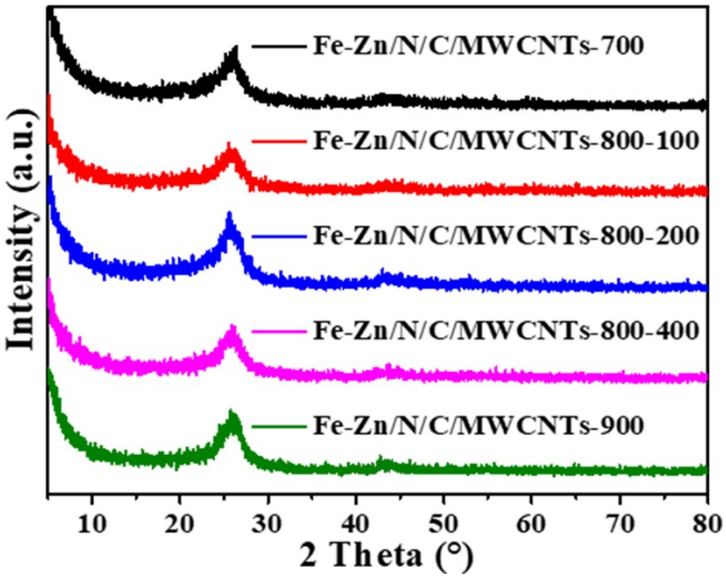

Fig. S3. XRD patterns of Fe-Zn/N/C/MWCNTs-700, Fe-Zn/N/C/MWCNTs-800-100, Fe-Zn/N/C/MWCNTs-800-200, Fe-Zn/N/C/MWCNTs-800-400, and Fe-Zn/N/C/MWCNTs-900.

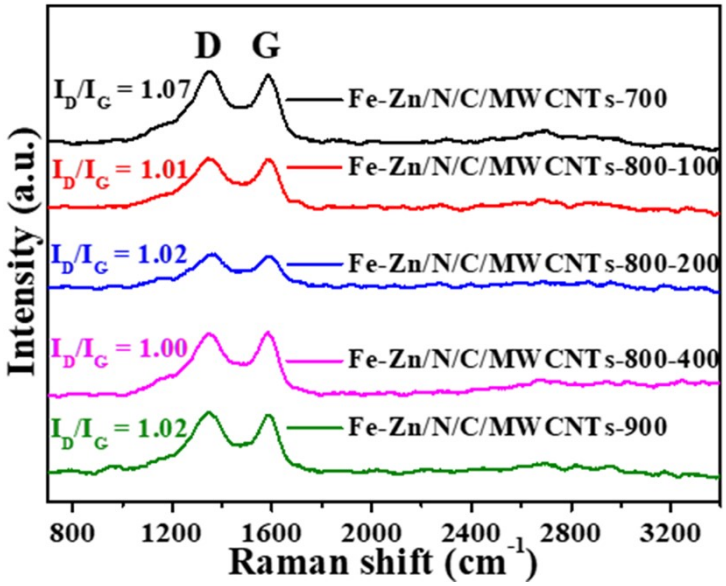

Fig. S4. Raman spectra of Fe-Zn/N/C/MWCNTs-700, Fe-Zn/N/C/MWCNTs-800-100, Fe-Zn/N/C/MWCNTs-800-200, Fe-Zn/N/C/MWCNTs-800-400, and Fe-Zn/N/C/MWCNTs-900.

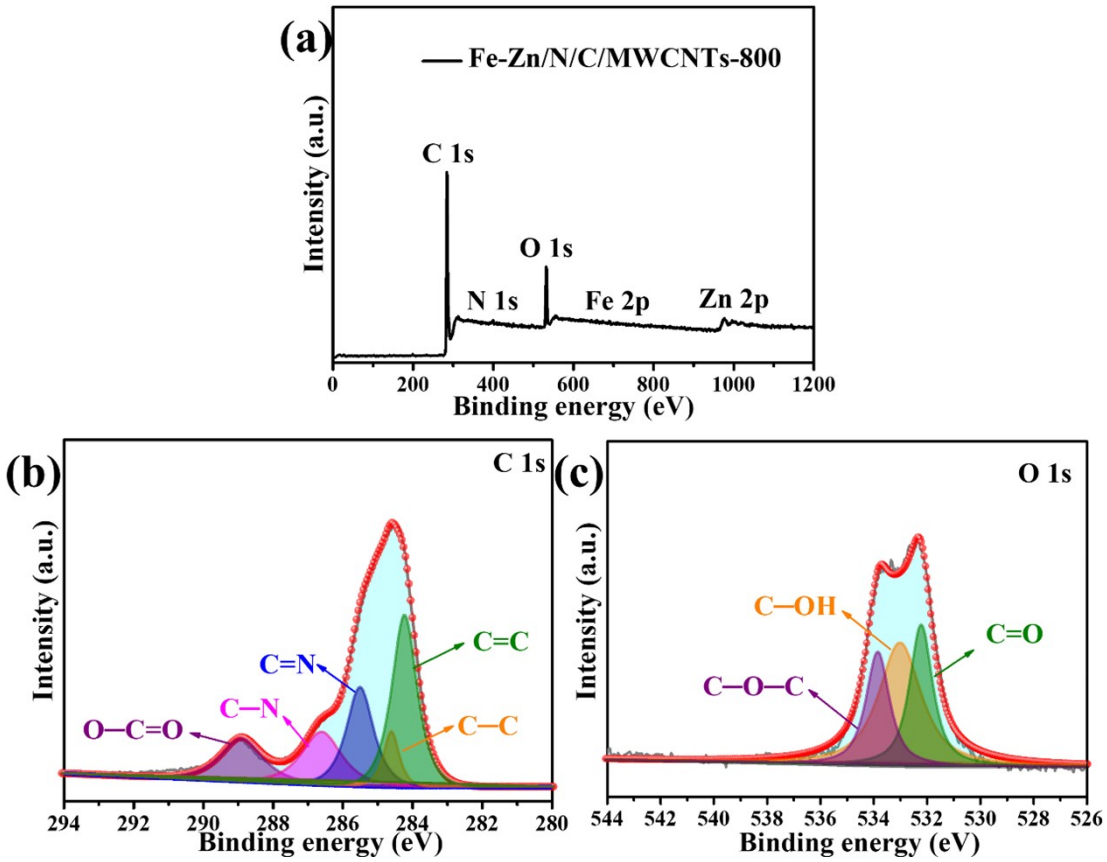

Fig. S5. High-resolution XPS spectra of Fe-Zn/N/C/MWCNTs-800 at (a) overall, (b) C 1s, and (c) O 1s region, respectively.

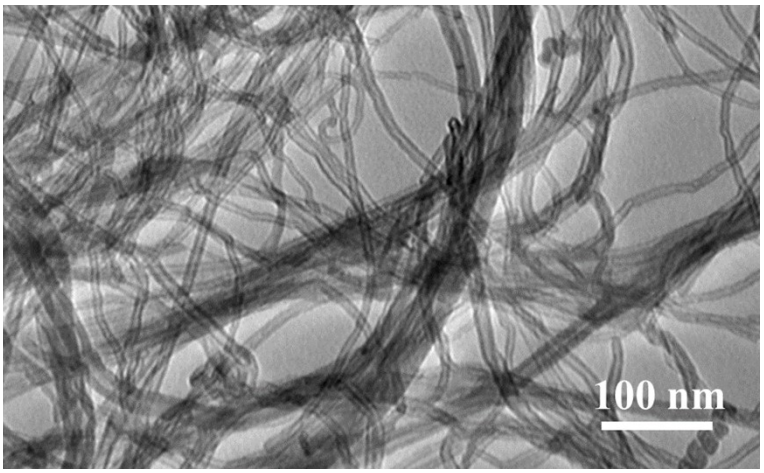

Fig. S6. TEM image of pure MWCNTs.

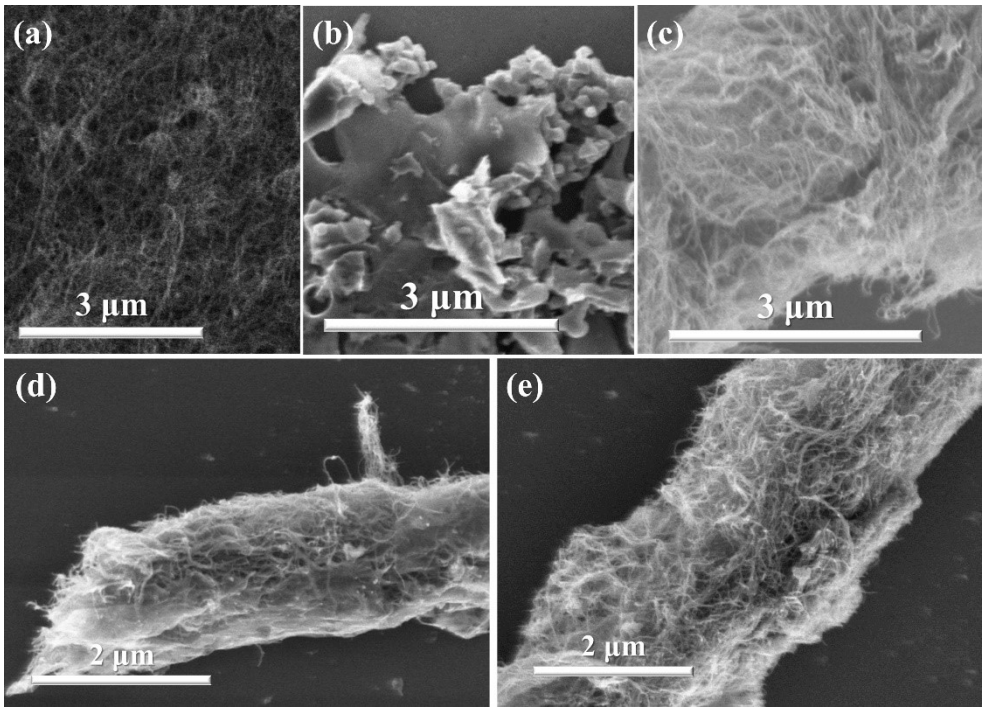

Fig. S7. SEM images of (a) MWCNTs, (b) Fe-Zn/N/C -800, (c) Fe-Zn/C/MWCNTs-800, (d) Fe-Zn/N/MWCNTs-800, and (e) Fe/N/C/MWCNTs-800.

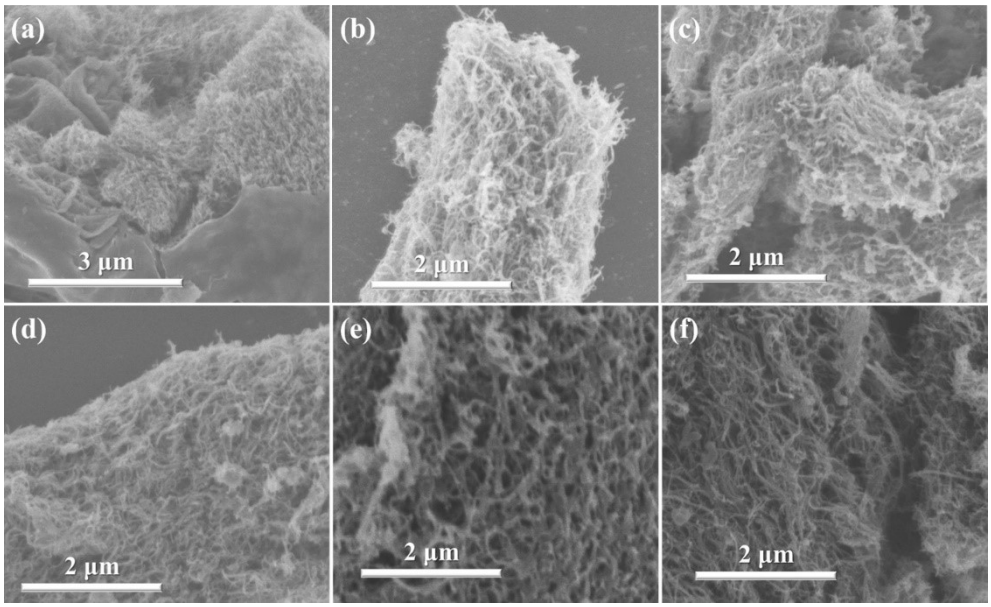

Fig. S8. SEM images of (a) Zn/N/C/MWCNTs-800, (b) Fe-Zn/N/C/MWCNTs-700, (c) Fe-Zn/N/C/MWCNTs-800-100, (d) Fe-Zn/N/C/MWCNTs-800-200, (e) Fe-Zn/N/C/MWCNTs-800-400, and (f) Fe-Zn/N/C/MWCNTs-900.

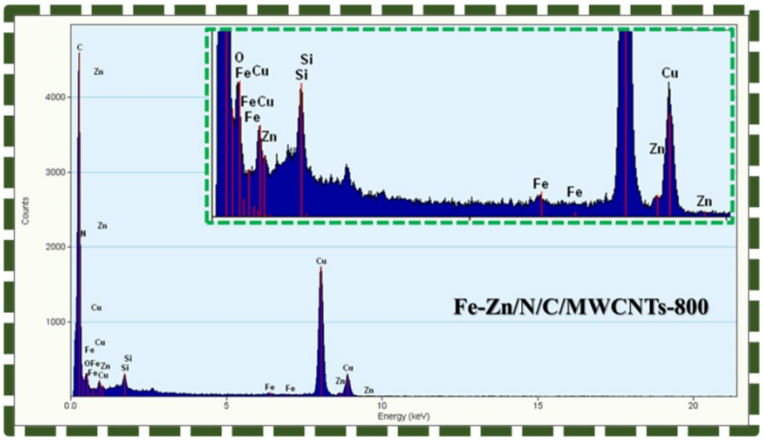

Fig. S9. EDX spectrum of Fe-Zn/N/C/MWCNTs-800.

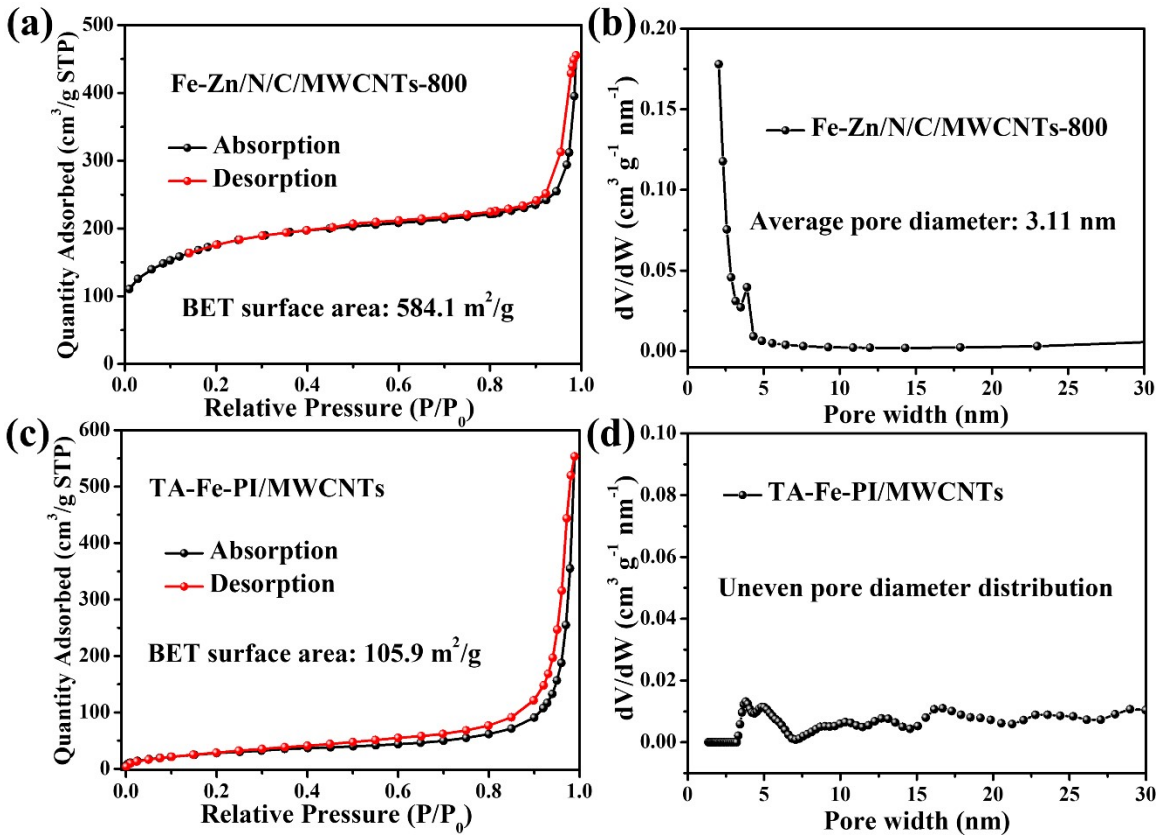

Fig. S10. (a) N_2 adsorption-desorption isotherms and (b) the corresponding pore distribution curves of Fe-Zn/N/C/MWCNTs-800. (c) N_2 adsorption-desorption isotherms and (d) the corresponding pore distribution curves of TA-Fe-PI/MWCNTs sample (before pyrolysis).

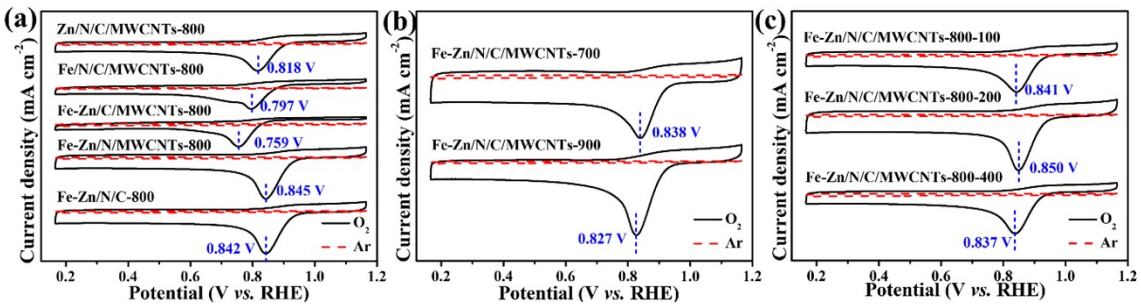

Fig. S11. Cyclic voltammetry (CV) curves of (a) Zn/N/C/MWCNTs-800, Fe/N/C/MWCNTs-800, Fe-Zn/N/MWCNTs-800, Fe-Zn/C/MWCNTs-800, and Fe-Zn/N/C-800, (b) Fe-Zn/N/C/MWCNTs-700 and Fe-Zn/N/C/MWCNTs-900, and (c) Fe-Zn/N/C/MWCNTs-800-100, Fe-Zn/N/C/MWCNTs-800-200, and Fe-Zn/N/C/MWCNTs-800-400 for ORR measured in Ar- and O_2- saturated 0.1 M KOH electrolyte.

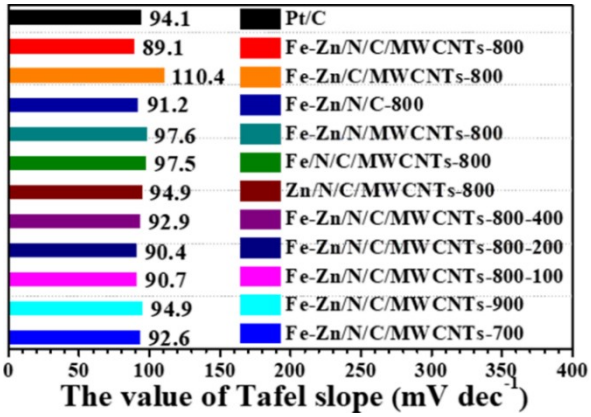

Fig. S12. The value of Tafel slope in this work.

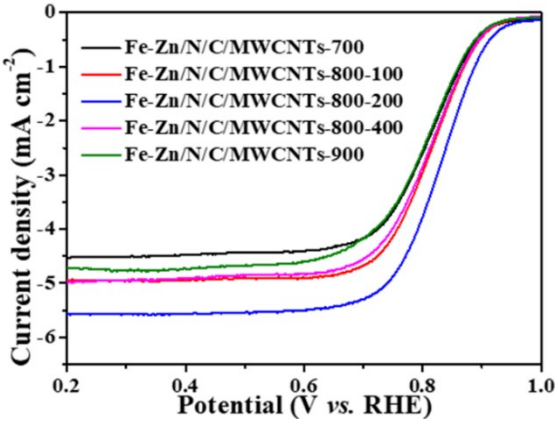

Fig. S13. Linear sweep voltammetry (LSV) curves of Fe-Zn/N/C/MWCNTs-700, Fe-Zn/N/C/MWCNTs-800-100, Fe-Zn/N/C/MWCNTs-800-200, Fe-Zn/N/C/MWCNTs-800-400, and Fe-Zn/N/C/MWCNTs-900.

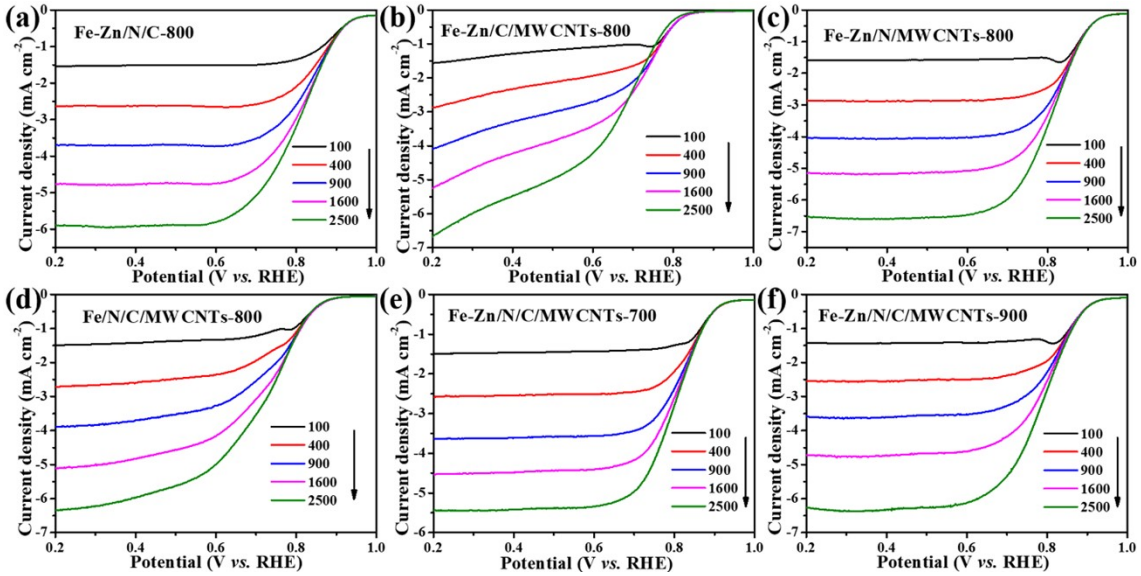

Fig. S14. LSV curves of (a) Fe-Zn/N/C-800, (b) Fe-Zn/C/MWCNTs-800, (c) Fe-Zn/N/MWCNTs-800, (d) Fe/N/C/MWCNTs-800, (e) Fe-Zn/N/C/MWCNTs-700, and (f) Fe-Zn/N/C/MWCNTs-900 at different rotation rates (from 100 rpm to 2500 rpm) with a scan rate of 10 $mV \cdot s^{-1}$ in O_2- saturated 0.1 M KOH electrolyte.

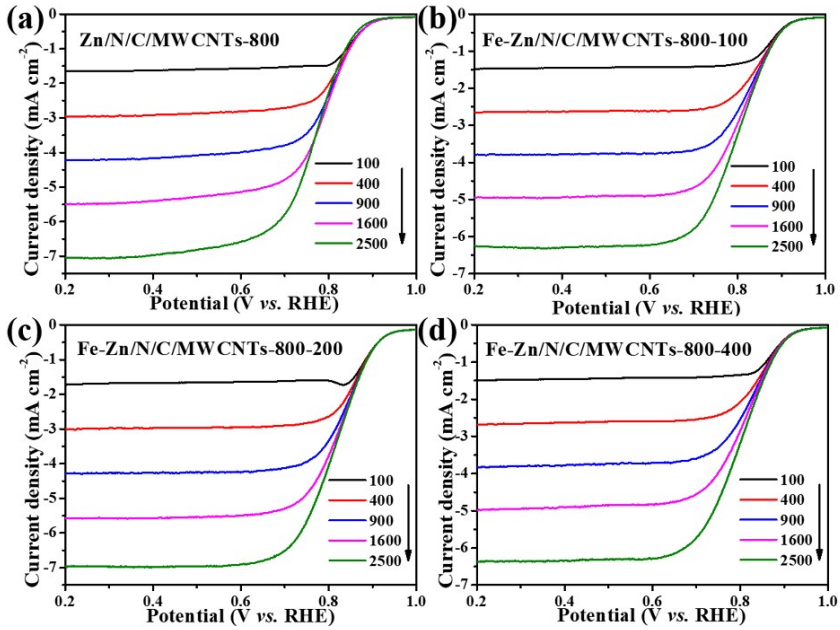

Fig. S15. LSV curves of (a) Zn/N/C/MWCNTs-800, (b) Fe-Zn/N/C/MWCNTs-800-100, (c) Fe-Zn/N/C/MWCNTs-800-200, and (d) Fe-Zn/N/C/MWCNTs-800-400 at different rotation rates (from 100 rpm to 2500 rpm) with a scan rate of 10 $mV \cdot s^{-1}$ in O_2- saturated 0.1 M KOH electrolyte.

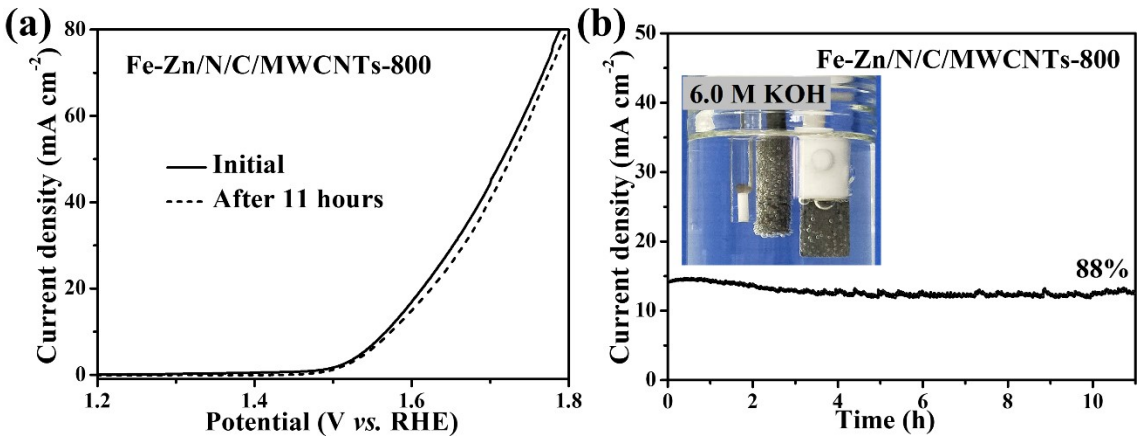

Fig. S16. (a) LSV curves of Fe-Zn/N/C/MWCNTs-800 catalyst before and after the stability testing toward OER. (b) Time-dependent current density curves of Fe-Zn/N/C/MWCNTs-800 on carbon paper for 11 hrs in 6.0 M KOH solutions.

Table S1. ICP-OES analysis results of the Fe-Zn/N/C/MWCNTs catalyst.

Catalyst	Fe (%)	Zn (%)
Fe-Zn/N/C/MWCNTs-800	0.38	0.24

Table S2. The ORR parameters compared with state-of-the-art catalysts and the performance of Zn-air batteries in the literature.

Catalysts	ORR	ZABs		Ref.
	$E_{1/2}$ (V *vs.* RHE)	Peak power density ($mW \cdot cm^{-2}$)	Stability (h)	
Fe-Zn/N/C/MWCNTs-800	0.858	259	180	This work
Fe-Zn-SA/NC	0.85	167.2	120	[1]
FeZnNC	0.873	170	110	[2]
Fe-N_4 SAs/NPC	0.885	232	36	[3]
(Zn, Co)/NSC	0.893	150	22	[4]
CuZn/NC	0.884	164.3	-	[5]
SA-Fe-NC	0.88	164	320	[6]
SA-Fe-NHPC	0.93	266.4	240	[7]
Fe@Fe_{SA}-N-C-900	0.83	110	500	[8]
FeCo SAs@Co/N-GC	0.88	207	200	[9]
Fe, Co-SA/CS	0.86	86.65	-	[10]
FeCo-1/NSC	0.82	162.74	150	[11]
FeCo-WC/NC	0.85	122.52	200	[12]
A-FeCo@NCNs	0.87	132	-	[13]
FeCo–N–C	0.904	196.3	77	[14]
CoFe–NC	0.94	115	80	[15]
NiFe-DG	0.86	148	-	[16]
Fe–Ni ANC@NSCA	0.891	140.3	500	[17]
Fe–NiNC-50	0.85	220	100	[18]
FeNi0.25-NC	0.86	180	8	[19]
Fe, Mn/N–C	0.928	160.8	81	[20]
Fe/Mn-N_x-C	0.88	208.6	18	[21]
Fe, Mn, N-FGC	0.89	220	-	[22]

Supplementary References

[1] J. Xu, S. Lai, D. Qi, M. Hu, X. Peng, Y. Liu, W. Liu, G. Hu, H. Xu, F. Li, C. Li, J. He, L. Zhuo, J. Sun, Y. Qiu, S. Zhang, J. Luo and X. Liu, *Nano Res.*, 2020, **14**, 1374-1381.
[2] S. Yang, X. Xue, C. Dai, X. Liu, Q. Yin, J. Lian, Y. Zhao, Y. Bu and G. Li, *Appl. Surf. Sci.*, 2021, **546**, 148934.
[3] Y. Pan, S. Liu, K. Sun, X. Chen, B. Wang, K. Wu, X. Cao, W.C. Cheong, R. Shen, A. Han, Z. Chen, L. Zheng, J. Luo, Y. Lin, Y. Liu, D. Wang, Q. Peng, Q. Zhang, C. Chen and Y. Li, *Angew. Chem. Int. Ed.*, 2018, **57**, 8614-8618.
[4] D. Liu, B. Wang, H. Li, S. Huang, M. Liu, J. Wang, Q. Wang, J. Zhang and Y. Zhao, *Nano Energy*, 2019, **58**, 277-283.
[5] D. Qi, Y. Liu, M. Hu, X. Peng, Y. Qiu, S. Zhang, W. Liu, H. Li, G. Hu, L. Zhuo, Y. Qin, J. He, G. Qi, J. Sun, J. Luo and X. Liu, *Small*, 2020, **16**, 2004855.
[6] X. Liang, Z. Li, H. Xiao, T. Zhang, P. Xu, H. Zhang, Q. Gao and L. Zheng, *Chem. Mater.*, 2021, **33**, 5542-5554.
[7] G. Chen, P. Liu, Z. Liao, F. Sun, Y. He, H. Zhong, T. Zhang, E. Zschech, M. Chen, G. Wu, J. Zhang and X. Feng, *Adv. Mater.*, 2020, **32**, 1907399.
[8] W. Zhang, K. Fan, C.-H. Chuang, P. Liu, J. Zhao, D. Qi, L. Zong and L. Wang, *J. Energy Chem.*, 2021, **61**, 612-621.
[9] N.K. Wagh, D.-H. Kim, S.-H. Kim, S.S. Shinde and J.-H. Lee, *ACS Nano*, 2021, **15**, 14683-14696.
[10] V. Jose, H. Hu, E. Edison, W. Manalastas Jr., H. Ren, P. Kidkhunthod, S. Sreejith, A. Jayakumar, J.M.V. Nsanzimana, M. Srinivasan, J. Choi and J.-M. Lee, *Small Methods*, 2021, **5**, 2000751.
[11] S. Chang, H. Zhang and Z. Zhang, *J. Energy Chem.*, 2021, **56**, 64-71.
[12] L. Xu, S. Wu, D. Deng, C. Wang, J. Qian, G. Lu and H. Li, *J. Alloys Compd.*, 2021, **868**, 159236.
[13] Y. Luo, J. Zhang, J. Chen, Y. Chen, C. Zhang, Y. Luo, G. Wang and R. Wang, *J. Catal.*, 2021, **397**, 223-232.
[14] D. Wang, H. Xu, P. Yang, X. Lu, J. Ma, R. Li, L. Xiao, J. Zhang and M. An, *J. Mater. Chem. A*, 2021, **9**, 13678-13687.
[15] K. Wang, J. Liu, Z. Tang, L. Li, Z. Wang, M. Zubair, F. Ciucci, L. Thomsen, J. Wright and N.M. Bedford, *J. Mater. Chem. A*, 2021, **9**, 13044-13055.
[16] K. Khan, X. Yan, Q. Yu, S.-H. Bae, J.J. White, J. Liu, T. Liu, C. Sun, J. Kim, H.-M. Cheng, Y. Wang, B. Liu, K. Amine, X. Pan and Z. Luo, *Nano Energy*, 2021, **90**, 106488.
[17] H. Li, X. Shu, P. Tong, J. Zhang, P. An, Z. Lv, H. Tian, J. Zhang and H. Xia, *Small*, 2021, **17**, 2102002.
[18] X. Zhu, D. Zhang, C.-J. Chen, Q. Zhang, R.-S. Liu, Z. Xia, L. Dai, R. Amal and X. Lu, *Nano Energy*, 2020, **71**, 104597.
[19] J. Liu, C. Fan, G. Liu and L. Jiang, *Appl. Surf. Sci.*, 2021, **538**, 148017.
[20] G. Yang, J. Zhu, P. Yuan, Y. Hu, G. Qu, B.A. Lu, X. Xue, H. Yin, W. Cheng, J. Cheng, W. Xu, J. Li, J. Hu, S. Mu and J.N. Zhang, *Nat. Commun.*, 2021, **12**, 1734.
[21] Z. Chen, X. Liao, C. Sun, K. Zhao, D. Ye, J. Li, G. Wu, J. Fang, H. Zhao and J. Zhang, *Appl. Catal. B*, 2021, **288**, 120021.
[22] S. Sarkar, A. Biswas, T. Purkait, M. Das, N. Kamboj and R.S. Dey, *Inorg. Chem.*, 2020, **59**, 5194-5205.